Supporting Information

All-Small-Molecule Ternary Organic Solar Cells with 16.26% Efficiency Enabled by Iodinated Electron Acceptor

Wenying Zhou[a], Jia Wang[a], Wendi Shi[b], Jiaying Wang[a], Shaohui Yuan[a], Baofa Lan[a], Bin Kan* [a]

[a] School of Materials Science and Engineering, National Institute for Advanced Materials, Nankai University, Tianjin, 300350, China.

[b] State Key Laboratory and Institute of Elemento-Organic Chemistry, Frontiers Science Center for New Organic Matter, The Centre of Nanoscale Science and Technology and Key Laboratory of Functional Polymer Materials, Renewable Energy Conversion and Storage Center (RECAST), College of Chemistry, Nankai University, Tianjin, 300071, China.

* Corresponding E-mails: kanbin04@nankai.edu.cn (B.K.).

Contents

1. General information

Unless stated otherwise, all solvents and reagents were received from commercial sources and used without further purification. BTR-Cl was purchased from Derthon Optoelectronics Materials Science Technology Co LTD, Y6 were purchased from Hyper Optoelectronics Materials and BO-4I was purchased Organtec Ltd.

2. Measurements and Instruments

UV-visible (UV-vis) absorption. UV-vis absorption spectra and Variable-temperature UV-vis absorption spectra were recorded on a Cary 5000 UV-vis spectrophotometer.

Fourier-transform photocurrent spectroscopy EQE (FTPS-EQE). The FTPS-EQE measurement was carried out on an Enlitech FTPS PECT-600 instrument. The optimal devices were used for FTPS-EQE measurement directly.

Atomic force microscopy (AFM). The AFM images were obtained from a Bruker Dimension Icon atomic force microscope by using in tapping mode. The film samples were prepared under the same conditions as those used for device fabrication.

Grazing incidence wide angle X-ray scattering (GIWAXS). The GIWAXS data were obtained at Xeuss 3.0 UHR Diffuse X-ray Scattering Station, Xenocs. The film samples on the Si substrate were prepared under the same conditions as those used for device fabrication.

Measurement of charge carrier mobilities. The hole and electron mobilities were measured by using space-charge-limited current (SCLC) method. Hole mobilities were measured with the device structure of ITO/3-BPIC-F/active layer/MoO_x/Ag. Electron mobilities were measured with the device structure of ITO/ZnO/active layer/PNDIT-F3N/Ag. The hole and electron mobilities estimated by the following equation: $J = 9\varepsilon_0\varepsilon_r\mu V^2/8d^3$, where J is the current density, ε_0 is the vacuum permittivity, ε_r is the relative dielectric constant, V is the internal voltage in the device, and d is the thickness of the active layer.

Transient photocurrent/photovoltage (TPC/TPV) Characterization Transient photocurrent (TPC) and photovoltage (TPV) measurements were performed on a Molex 180081-4320 with light intensity about 0.5 sun, Voltage and current dynamics were recorded on a digital oscilloscope (Tektronix MDO4104C). Voltages at open circuit and currents under short circuit conditions were measured over a 1 MΩ and a 50 Ω resistor, respectively.

Contact Angles Measurements. The contact angles of two different solvents (water and glycerol) on the neat films (donor/acceptor) were measured on a JC2000D1 drop shape analyzer (POWEREACH®). The miscibility of two components in the blend can

be estimated from the solubility parameters (δ) of each material, which can be calculated with equation: $\delta = K\sqrt{\gamma}$, Where γ is the surface energy of the material, and K is the proportionality constant ($K = 116 \times 10^3$ m$^{1/2}$).[1]

***E*loss Analysis**. The following equation was used to quantify the E_{loss} of OSCs:[2]

$$E_{loss} = E_g^{PV} - qV_{oc} = \left(E_g^{PV} - qV_{oc}^{SQ}\right) + \left(qV_{oc}^{SQ} - qV_{oc}^{rad}\right) + \left(qV_{oc}^{rad} - qV_{oc}\right) = \Delta E_1 + \Delta E_2 + \Delta E_3$$

E_g^{PV} represents the bandgap of the blend film and q is the elementary charge. E_g^{PV} can be estimated via the derivatives of the sensitive EQE (EQE_{PV}) spectra(P(E)=dEQE/dE) as following:

$$E_g^{PV} = \frac{\int_a^b E_g \mathrm{P}(E_g)\mathrm{d}E_g}{\int_a^b \mathrm{P}(E_g)\mathrm{d}E_g}$$

where the integration limits a and b are chosen as the energy where P(E_g) is equal to 50% of its maximum. The EQE_{PV} measurements were conducted on an Enlitech FTPS PECT-600 instrument. The total E_{loss} can be divided into three parts:

(1) $\Delta E_1 = E_g - qV_{oc}^{SQ}$ represents the unavoidable radiative loss originating from absorption above the bandgap. The V_{oc}^{SQ} is the maximum voltage based on the Shockley–Queisser (SQ) limit:

$$V_{oc}^{SQ} = \frac{kT}{q}\ln\left(\frac{J_{sc}^{SQ}}{J_0^{SQ}} + 1\right) \cong \frac{kT}{q}\ln\left(\frac{q\cdot\int_{E_g}^{+\infty}\phi_{AM1.5G}(E)\mathrm{d}E}{q\cdot\int_{E_g}^{+\infty}\phi_{BB}(E)\mathrm{d}E}\right)$$

(2) $\Delta E_2 = qV_{oc}^{SQ} - qV_{oc}^{rad}$ can be regarded as radiative loss caused by absorption below the bandgap, where the V_{oc}^{rad} is the open circuit voltage when there is only radiative recombination. The radiative recombination limit for the saturation current (J_0^{rad}) is also calculated from the EQE spectrum:

$$V_{oc}^{rad} = \frac{kT}{q}\ln\left(\frac{J_{sc}}{J_0^{rad}} + 1\right) \cong \frac{kT}{q}\ln\left(\frac{q\cdot\int_0^{+\infty}\mathrm{EQE}(E)\phi_{AM1.5G}(E)\mathrm{d}E}{q\cdot\int_0^{+\infty}\mathrm{EQE}(E)\phi_{BB}(E)\mathrm{d}E}\right)$$

where q is the elementary charge and ϕ_{BB} is the black body spectrum at 300 K.

(3) $\Delta E_3 = qV_{oc}^{rad} - qV_{oc}$ can be directly calculated while the other two parts were determined. ΔE_3 can also be confirmed by measuring the EQE of electroluminescence

(EQE_{EL}) of the solar cell through the equation of: ΔE_3=-kT ln(EQE_{EL}). For the EQE_{EL} measurements, a digital source meter (Keithley 2400) was 80 employed to inject electric current into the solar cells, and the emitted photons were collected by a Si diode (Hamamatsu s1337-1010BQ) and indicated by a picoammeter (Keithley 6482).

3. Device Fabrication and Characterization

OPV device fabrication. The OSCs were fabricated with a conventional structure of ITO/3-BPIC-F/Active layer/PNDIT-F3N/Ag. First, ITO-coated glass was cleaned with deionized water, acetone, and isopropyl alcohol under ultrasonication for sequentially 10 min. Second, the surface of ITO-coated glass was treated in an ultraviolet-ozone chamber for 15 min. A thin layer of 3-BPIC-F was deposited on the ITO substrate at 3000 rpm for 20 s and then dried at 100 °C for 10 min in air. Then the substrates were transferred to a glovebox filled with nitrogen. The active layer solutions of BTR-Cl:Y6 (1.8:1) and BTR-Cl:Y6:BO-4I (1.8:0.95:0.05) were dissolved in chloroform (the total concentration of blend solutions was 23 mg mL^{-1} for both blends) with 0.25 vol% 1,8-diiodooctane (DIO). The solution was stirred at 85 ℃ for 2 h in a nitrogen-filled glove box. The active layer was spun onto the 3BPIC-F layer at 2500 rpm for 20 s, and then the films were treated with thermal annealing at 140 °C for 8 min. After cooled down, the methanol solution of PNDIT-F3N (1 mg/mL) was spin-coated on the top of the active layer at 3300 rpm for 20 s. Finally, an Ag electrode with a thickness of 120 nm was evaporated under a vacuum of 1×10^{-4} Pa. The active area of the device was 0.04 cm^2, and a shadow mask with an area of 0.0324 cm^2 was utilized during the *J-V* testing.

The glue dispenser/spin coater (Brand-REESEEN, PvS-mini7) used in the lab are from Jiangyin J. Wanjia Technology Co., Ltd.

OPV devices characterization. The current density-voltage (*J-V*) curves of OSCs were recorded on a Keithley 2400 source-measure unit in a glove box filled with nitrogen. Enli SS-F5-3A solar simulator with AM 1.5 G was used as the light source, and the light intensity was 100 mW cm^{-2} which was calibrated by a standard Si solar cell (made by Enli Technology Co., Ltd., Taiwan, and calibrated report can be traced to NREL). A QE-R Solar Cell Spectral Response Measurement System was used to measure the external quantum efficiency (EQE) values of the devices. A Veeco Dektak 150 profilometer was used to measure the thickness of the active layers.

4. Supporting Figures and Tables

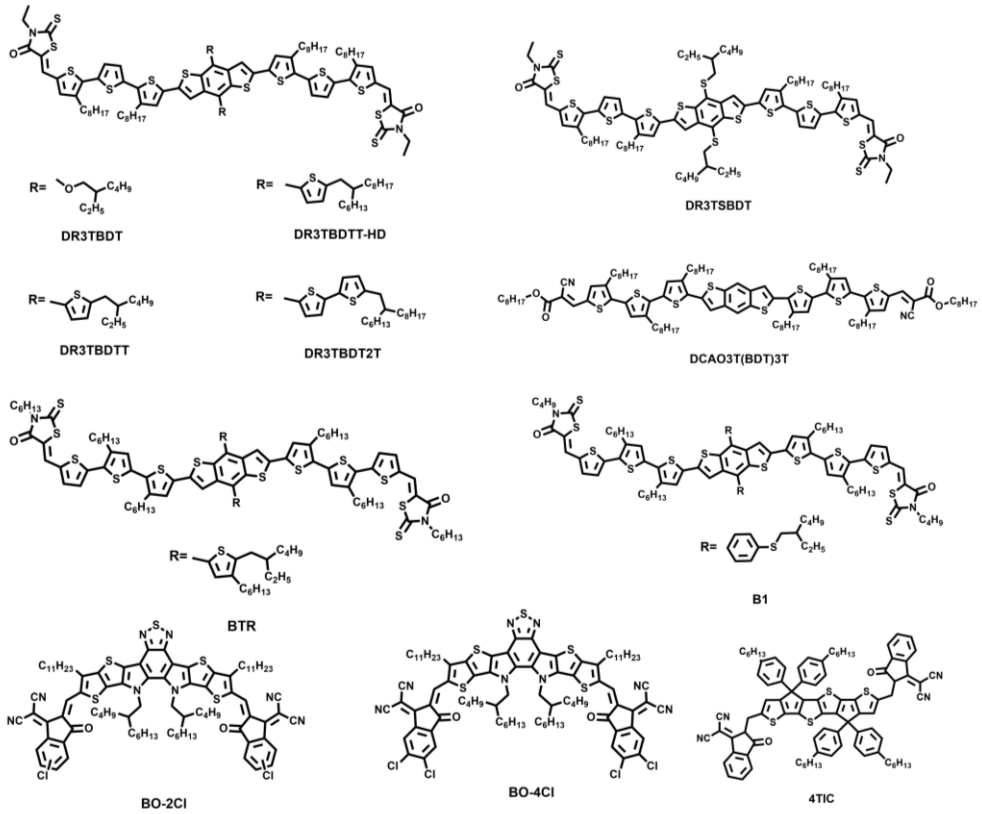

Figure S1. The chemical structures of the corresponding small-molecule donors and acceptors mentioned in the Introduction part.

Table S1 Summary of the GIWAXS parameters for the BTR-Cl, Y6, and BO-4I films.

Neat Films	In-Plane Lamellar stacking				Out-of-Plane π-π stacking			
	q **(Å^{-1})**	***d*-spacing (Å)**[a]	**FWHM (Å)**	**CL (Å)**[b]	***q*** **(Å^{-1})**	***d*-spacing (Å)**[a]	**FWHM (Å)**	**CL (Å)**[b]
BTR-Cl	0.35	17.95	0.06	94.24	1.56	4.03	4.42	1.28
Y6	0.30	20.94	0.05	113.09	1.79	3.51	0.15	37.70
BO-4I	0.43	14.61	0.10	56.54	1.71	3.67	0.39	14.50

[a] Calculated from the equation: d-spacing = $2\pi/q$.

[b] Obtained from the Scherrer equation: CL = 2 πK/FWHM, where FWHM is the full-width at half-maximum and K is a shape factor (K = 0.9 here).

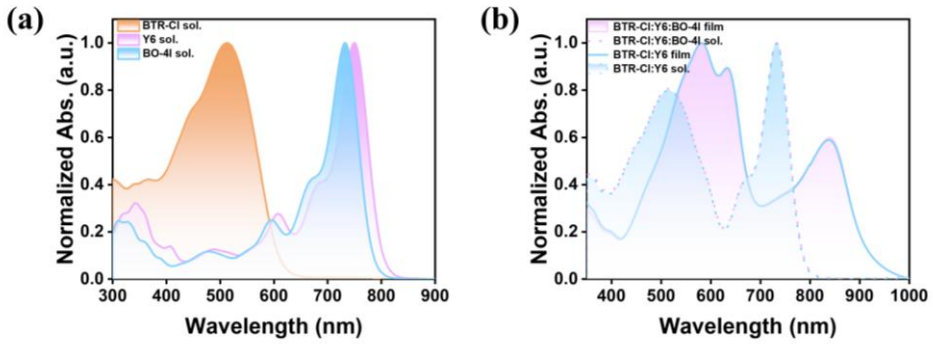

Figure S2. (a) Solution absorption spectra of BTR-Cl, Y6 and BO-4I. (b) Solution and film absorption of BTR-Cl:Y6 and BTR-Cl:Y6:BO-4I.

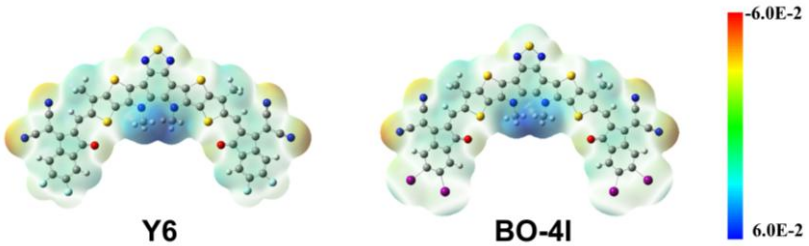

Figure S3. Electrostatic potential (ESP) distributions of Y6 and BO-4I.

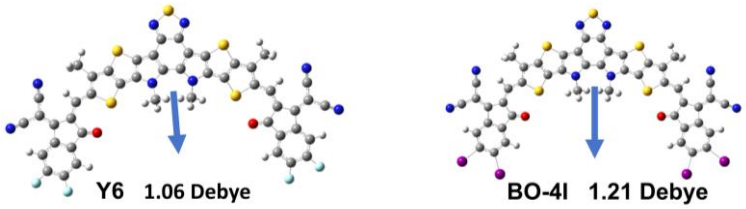

Figure S4. Molecular dipole of Y6 and BO-4I based on the density functional theory (DFT) calculation.

Table S2. Device optimization of BTR-Cl:BO-4I based binary devices.

BHJ	D:A	V_{oc} (V)	J_{sc} (mA cm^{-2})	FF (%)	PCE$_{max}$ (%)
BTR-Cl:BO-4I	1.3:1	0.912	20.25	50.62	9.35
	1.5:1	0.909	19.60	51.24	9.13
	1.7:1	0.928	20.27	55.78	10.53
	1.8:1	0.921	19.95	54.67	10.13
	2.0:1	0.919	20.31	50.81	9.48

Table S3. Device optimization of BTR-Cl:Y6 based binary devices.

BHJ	D:A	V_{oc} (V)	J_{sc} (mA cm^{-2})	FF (%)	PCE$_{max}$ (%)
BTR-Cl:Y6	1.3:1	0.801	24.35	66.10	13.00
	1.5:1	0.844	24.77	69.58	14.59
	1.8:1	0.844	25.78	70.93	15.43
	2.0:1	0.831	24.25	71.82	14.62

Table S4. Device optimization of BTR-Cl:Y6:BO-4I based binary devices.

BHJ	D:A	V_{oc} (V)	J_{sc} (mA cm^{-2})	FF (%)	PCE$_{max}$ (%)
BTR-Cl:Y6:BO-4I	1.8:1:0.1	0.812	25.56	68.10	14.16
	1.8:0.975:0.025	0.844	24.77	69.58	14.59
	1.8:0.95:0.05	0.845	25.87	74.41	16.26
	1.8:0.9:0.1	0.840	25.61	70.30	15.30
	1.8:0.8:0.2	0.864	24.46	68.23	14.41
	1.8:0.7:0.3	0.888	23.18	60.95	12.59

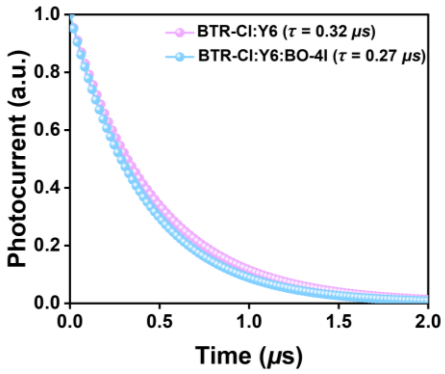

Figure S5. TPC curves of binary and ternary ASM-OSCs.

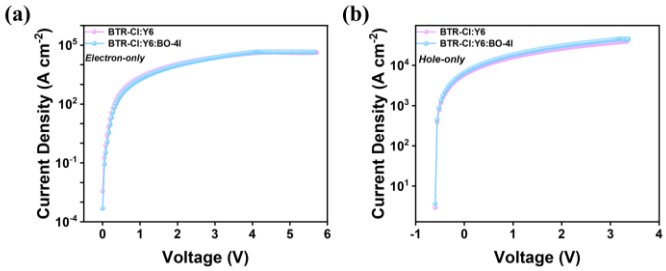

Figure S6. (a) Electron and (b) hole mobility curves based on electron-only and hole-only devices.

Table S5. The hole and electron mobilities of the binary and ternary devices.

Active layer	μ_h ($\times10^{-4}$ cm^2 V^{-1} s^{-1})	μ_e ($\times10^{-4}$ cm^2 V^{-1} s^{-1})	μ_h/μ_e
BTR-Cl:Y6	6.57	4.55	1.44
BTR-Cl:Y6:BO-4I	7.34	5.15	1.42

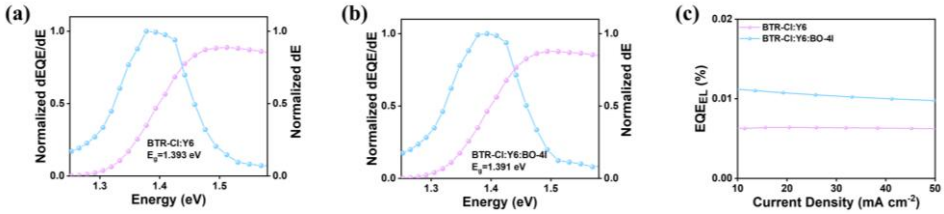

Figure S7. Optical bandgap determination of (a) BTR-Cl:Y6 and (b) BTR-Cl:Y6:BO-4I based on the derivatives of the *EQE* spectra. The region between two lines is the part where the gap distribution probability is greater than half of the maximum, which is used for the bandgap calculation. (c) EQE_{EL} curves of BTR-Cl:Y6 and BTR-Cl:Y6:BO-4I based ASM-OSCs.

Table S6. Detailed energy loss parameters of the ASM-OSCs.

Active layer	E_g (eV)	qV_{oc} (eV)	E_{loss} (eV)	ΔE_1 (eV)	ΔE_2 (eV)	ΔE_3[a] (eV)	EQE_{EL} (%)	ΔE_3[b] (eV)
BTR-Cl:Y6	1.393	0.844	0.549	0.263	0.064	0.222	6.62×10^{-3}	0.250
BTR-Cl:Y6: BO-4I	1.391	0.845	0.546	0.263	0.063	0.220	1.04×10^{-2}	0.237

ΔE_3^b is calculated from the EQE_{EL} measurements.

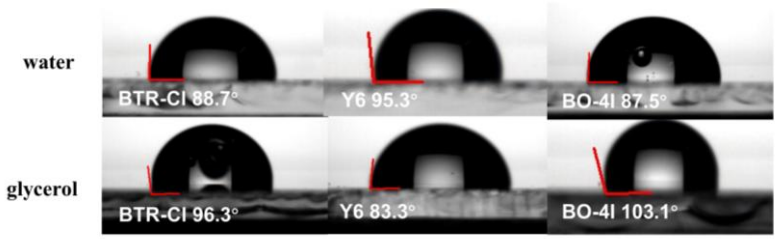

Figure S8. Contact angle images of water and glycerol droplets on the neat films.

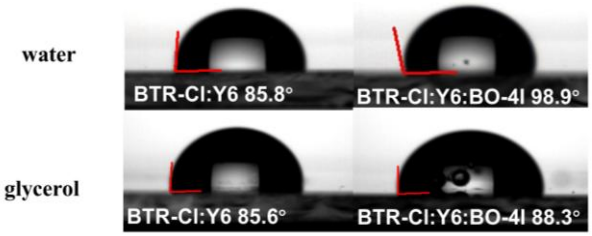

Figure S9. Contact angle images of water and glycerol droplets on BTR-Cl:Y6 and BTR-Cl:Y6:BO-4I blend films.

Table S7. Key parameters of contact angle measurements by using water and glycerol.

Sample	Contact angles		γ (mN m^{-1})	$\chi^{A\text{-}D}$ (K)	$\chi^{D_1\text{-}D_2}$ (K)
	θ_{water} (°)	$\theta_{glycerol}$ (°)			
BTR-Cl	88.7	96.3	26.4	/	/
Y6	95.3	83.3	32.9	0.35	/
BO-4I	103.1	87.5	29.7	0.10	0.08

Table S8. Summary of the GIWAXS parameters for the BTR-Cl:Y6 and BTR-Cl:Y6:BO-4I blend films.

Blend Films	In-Plane (010) Lamellar stacking				Out-of-Plane π-π stacking			
	q (Å^{-1})	*d*-spacing (Å)[a]	FWHM (Å)	CL (Å)[b]	*q* (Å^{-1})	*d*-spacing (Å)[a]	FWHM (Å)	CL (Å)[b]
BTR-Cl:Y6	0.34	18.47	0.05	113.09	1.82	3.45	0.08	80.78
BTR-Cl:Y6: BO-4I	0.35	17.95	0.05	113.09	1.83	3.43	0.06	94.24

[a] Calculated from the equation: d-spacing = $2\pi/q$.

[b] Obtained from the Scherrer equation: CL = 2 πK/FWHM, where FWHM is the full-width at half-maximum and K is a shape factor (K = 0.9 here).

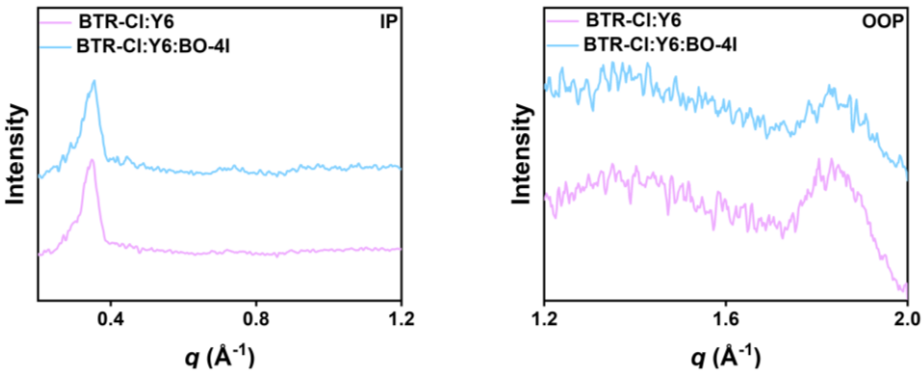

Figure S10. The corresponding IP and OOP line-cut profiles for two blend films.

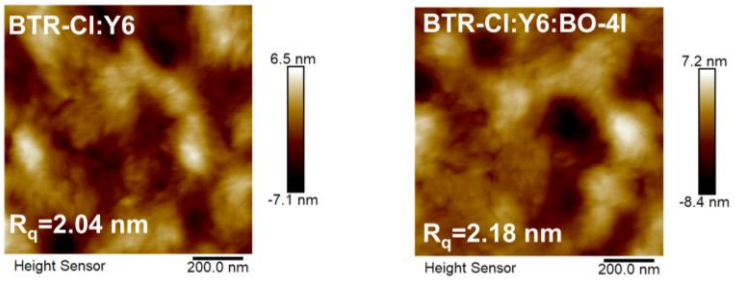

Figure S11. AFM height images for BTR-Cl:Y6 and BTR-Cl:Y6:BO-4I blend films, respectively.

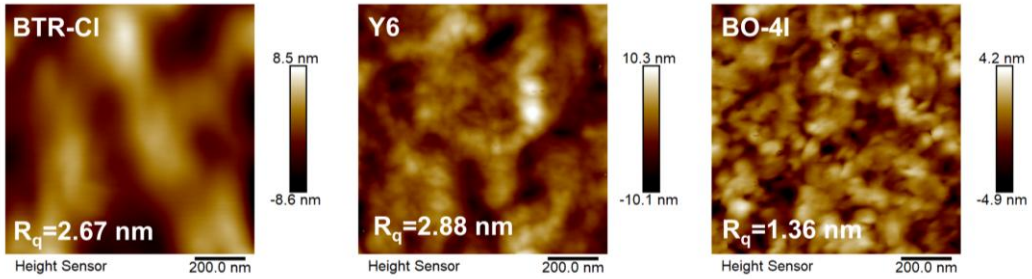

Figure S12. AFM height images for BTR-Cl, Y6 and BO-4I neat films, respectively.

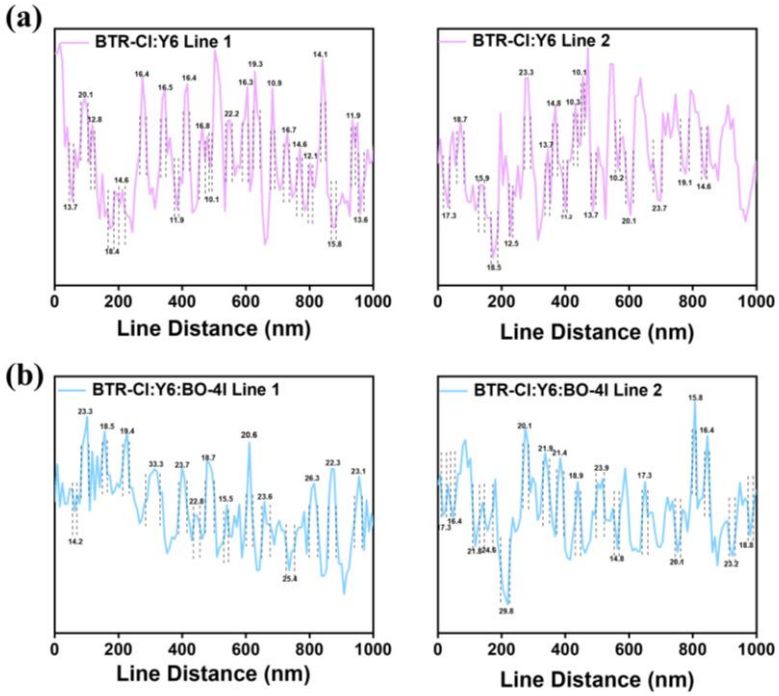

Figure S13. Fibril diameter diagrams of (a) BTR-Cl:Y6 and (b) BTR-Cl:Y6:BO-4I blend films, respectively.

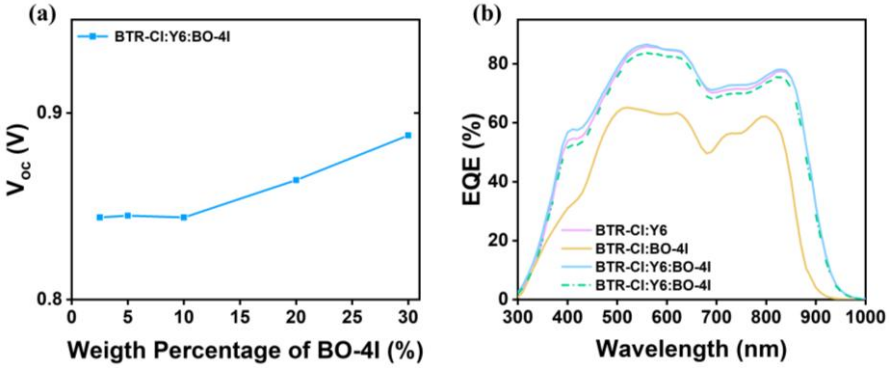

Figure S14. (a) V_{oc} as a function of BO-4I weight percentage in BTR-Cl:Y6:BO-4I ternary devices. (b) EQE spectra of BTR-Cl:Y6(pink line), BTR-Cl:BO-4I (yellow line); The experimental (blue solid line) and calculated (green dashed line) EQE spectra for the BTR-Cl:Y6:BO-4I ternary devices, respectively. The calculated spectrum was obtained based on the weighted average of the EQE spectra from the two binary devices.

References

1. J. Wang, P. Wang, T. Chen, W. Zhao, J. Wang, B. Lan, W. Feng, H. Liu, Y. Liu, X. Wan, G. Long, B. Kan and Y. Chen, *Angewandte Chemie International Edition*, 2025, **64**, e202423562.
2. H. Xia, Y. Zhang, W. Deng, K. Liu, X. Xia, C. J. Su, U. S. Jeng, M. Zhang, J. Huang, J. Huang, C. Yan, W. Y. Wong, X. Lu, W. Zhu and G. Li, *Advanced Materials*, 2022, **34**, 2107659.